Received: 20 March 2022 | Revised: 8 February 2023 | Accepted: 14 February 2023

DOI: 10.1111/pce.14573

ORIGINAL ARTICLE

Plant, Cell & Environment | WILEY

Xylem resistance to cavitation increases during summer in *Pinus halepensis*

Feng Feng[1,2] | Yael Wagner[3] | Tamir Klein[3] | Uri Hochberg[1]

[1]Institute of Soil, Water and Environmental Sciences, Volcani Center, Agricultural Research Organization, Rishon LeZion, Israel

[2]Department of Botany, University of Innsbruck, Innsbruck, Austria

[3]Department of Plant and Environmental Sciences, Weizmann Institute of Science, Rehovot, Israel

Correspondence
Uri Hochberg, Institute of Soil, Water and Environmental Sciences, Volcani Center, Agricultural Research Organization, Rishon LeZion 7505101, Israel.
Email: Hochberg@agri.gov.il

Funding information
Israel Science Foundation

Abstract

Cavitation resistance has often been viewed as a relatively static trait, especially for stems of forest trees. Meanwhile, other hydraulic traits, such as turgor loss point (Ψ_{tlp}) and xylem anatomy, change during the season. In this study, we hypothesized that cavitation resistance is also dynamic, changing in coordination with Ψ_{tlp}. We began with a comparison of optical vulnerability (OV), microcomputed tomography (μCT) and cavitron methods. All three methods significantly differed in the slope of the curve,Ψ_{12} and Ψ_{88}, but not in Ψ_{50} (xylem pressures that cause 12%, 88%, 50% cavitation, respectively). Thus, we followed the seasonal dynamics (across 2 years) of Ψ_{50} in *Pinus halepensis* under Mediterranean climate using the OV method. We found that Ψ_{50} is a plastic trait with a reduction of approximately 1 MPa from the end of the wet season to the end of the dry season, in coordination with the dynamics of the midday xylem water potential (Ψ_{midday}) and the Ψ_{tlp}. The observed plasticity enabled the trees to maintain a stable positive hydraulic safety margin and avoid cavitation during the long dry season. Seasonal plasticity is vital for understanding the actual risk of cavitation to plants and for modeling species' ability to tolerate harsh environments.

KEYWORDS
cavitation resistance, *Pinus halepensis*, seasonality, turgor loss point, vulnerability curves

1 | INTRODUCTION

One of the major risks to plants under drought is hydraulic failure (Brodribb and Cochard 2009; Kursar et al., 2009; McDowell et al., 2008). As the soil dries and/or evaporative demand increases, negative pressure (Ψ_x) develops in the xylem. When this pressure exceeds the 'air seeding' threshold, a cavitation event occurs. An air bubble is pulled into a conduit, rapidly expands, and embolises it (Tyree and Zimmermann 2002). In the case of extensive levels of embolism, the plant faces desiccation of organs (Brodribb et al., 2021; Cardoso et al., 2020) and even death (Hammond et al., 2019). From a practical standpoint, the xylem pressure at which 50% loss of conductivity (LC) occurs (Ψ_{50}) has been found to correlate with drought resistance, and it is commonly used to determine plants' drought adaptation (Brodribb and Cochard 2009; Choat et al., 2012).

Many studies measured the plasticity of Ψ_{50} in response to environmental factors. Xylem vulnerability varied in respect to the light conditions (Lemoine et al., 2002; Schoonmaker et al., 2010), nutrients availability (Harvey and Driessche 1997, 1999; Beikircher et al., 2019; Bucci et al., 2006; Ewers et al., 2000; Hacke et al., 2010; Plavcová and Hacke 2012; Plavcová et al., 2013; Villagra et al., 2013), temperature variations (Mayr et al., 2002), and water availability

(Anderegg 2015; Awad et al., 2010; Beikircher and Mayr 2009; Cardoso et al., 2018; Jacobsen et al., 2007; Ladjal et al., 2005; Martorell et al., 2015; Stiller 2009). Despite this well-established plasticity, Ψ_{50} is considered a static trait through time, probably because the xylem is composed of dead cells and is thus less plastic once formed (Choat et al., 2012). The commonness of this perception is manifested by many studies which measured the xylem vulnerability curve (VC) at one point of the experiment and compared it with the seasonal dynamics of Ψ_x to determine if cavitation had taken place (e.g., Fontes et al., 2018; Hochberg et al., 2016; Skelton et al., 2017).

However, there are good reasons to assume that Ψ_{50} is, in fact, seasonally dynamic. For starters, most hydraulic traits will change during the season. Xylem architecture (the probable mechanistic determinant of Ψ_{50}; von Arx et al. 2012; Kaack et al., 2021), the turgor loss point (Ψ_{tlp}, which is normally coordinated with Ψ_{50}; Bartlett et al., 2014; Brodribb et al., 2003; Cardoso et al., 2018), and the stomatal closure (Herrera et al., 2022; Sorek et al., 2021) in respect to Ψ_x were shown to change during the season. Also, from a strategic point of view, a seasonal adjustment of stomatal closure and Ψ_{tlp} to lower Ψ_x will place plants at greater risk of cavitation unless an equal adjustment of Ψ_{50} takes place. Finally, the few studies that did characterize the seasonal dynamics of Ψ_{50} measured considerable seasonal plasticity.

Kolb and Sperry (1999) found that *Artemisia tridentata* reduced its Ψ_{50} from −1.6 MPa to −4.5 MPa from May to July. In addition, Jacobsen et al. (2007, 2014) found a 1–2 MPa decline in vulnerability to cavitation from the wet season to the dry season in several Californian plant species. More recently, grapevine shoots and leaves were shown to exhibit a 0.7–1 MPa decrease in Ψ_{50} as the growing season progressed (Charrier et al., 2018; Sorek et al., 2021), and similar patterns were also measured in leaves of other Mediterranean species (Sorek et al., 2022). It is difficult to understand if these examples are exceptions or the rule for most species. Specifically, a seasonal dynamic in a deciduous species, which grows its new functional xylem in a few months, seems more reasonable than equivalent plasticity in long-standing evergreen forest trees. Forest trees in general, and pines in particular, are known to have limited Ψ_{50} plasticity when grown under variable environments (Maherali and Delucia 2000; Klein et al., 2013; Ladjal et al., 2005; Lamy et al., 2014; Unterholzner et al., 2020), though they showed plasticity in some occasions (Domec et al., 2010; Corcuera et al., 2011; López et al., 2013).

In the current study, we examined the seasonal dynamics of cavitation resistance in stems of *Pinus halepensis*. Since pines are one of the most globally dominant forest species, the existence or lacking of a dynamic Ψ_{50} in pines would significantly impact our understanding of forests' response to drought. If pines seasonally acclimate their Ψ_{50} to lower values, then many of the studies that measured Ψ_{50} only at the wet season may have overestimated forest vulnerability to drought. We evaluated the cavitation resistance using the optical vulnerability (OV) method. We determined the accuracy of the OV measurement for pines' shoots through comparison with two established methods: microcomputed tomography (μCT; Brodribb et al., 2016; Choat et al., 2015; Cochard et al., 2015) and the cavitron (Cochard 2002; Cochard et al., 2005). We hypothesized that the xylem vulnerability is a seasonally plastic trait, which will adjust to lower Ψ_x along the summer in coordination with the known dynamics of the midday water potential (Ψ_{midday}) and the Ψ_{tlp}.

2 | MATERIALS AND METHODS

2.1 | Plant material and experimental design

The study consisted of two parts: (1) a comparison of OV method with the cavitron and μCT methods in pines' shoots, and (2) a characterization of the seasonal dynamics of the stems' Ψ_{midday}, xylem vulnerability, and Ψ_{tlp}.

2.1.1 | Experiment 1—methods comparison

Because of the controversies regarding the validity of methods for the assessment of xylem vulnerability (Choat et al., 2010; Wheeler et al., 2013), we decided to compare the OV method with more commonly used methods. VC of *P. halepensis* were constructed in June 2020 using three different methods: cavitron, μCT, and OV. The latter two are imaging methods, while the cavitron is a hydraulic method. Shoots were collected from three 2-year-old, 1.5 m tall, potted pines, growing in the greenhouse of Weizmann Institute of Science, Rehovot, Israel. Pines were watered daily in the morning to full capacity and kept under natural conditions. Five shoots were sampled for cavitron, 1–2 shoots per tree. Additional three branched shoots were sampled from each plant respectively for simultaneous evaluation using the OV and μCT. OV was continuously measured on 4–5 mm-thick twigs, while 1–2 mm-thick twigs from the same shoots were sampled every few hours and scanned using the μCT. The use of many samples from the same individual plants and the concurrent evaluation of multiple methods meant that we were not able to standardize sample size and location across methods. This may complicate a simple interpretation of these results.

2.2 | Cavitron method

The Cavitron technique (Cochard 2002; Cochard et al., 2005) is considered reliable for tracheid-bearing species such as conifers without the influence of the 'open vessel' artifact (Pivovaroff et al., 2016). It uses centrifugal force to generate Ψ_x in the xylem by spinning stem samples. The stems are exposed to stepwise decreasing Ψ_x, while measuring the conductivities at the same time. The VCs are plotted as the relationship between Ψ_x and the corresponding LC.

Shoots with a length of 70–80 cm were harvested, wrapped in wet tissue and placed in a black plastic bag, and transferred to the laboratory. Starting at approximately 20 cm from the apex, a 27.4 cm-long segment per shoot was then excised by carrying out several cuttings under water, debarked to minimize resin exudation, and both ends trimmed with a fresh razor blade (Delzon et al., 2010).

The 27.4-cm-long stem segment was fixed on a custom-built rotor (Cochard 2002) mounted on a Sorvall RC5 centrifuge (DuPont Instruments). Both ends of the segment were placed in plastic cuvettes filled with a solution that could be replenished. The solution is ultra-pure and degassed water, including 10 mM KCl and 1 mM $CaCl_2$. A positive hydrostatic pressure (ΔP), generated by different amounts of water in the two cuvettes, drove the water flow through the segment while spinning. The flow rate (F) was calculated by the amount of water moved at a given time interval. Then, the xylem specific conductivity (K_s) was calculated as:

$$K_s = \frac{F}{\Delta P} \frac{L}{A} \quad (1)$$

where L was the length and A was the xylem area of the segment.

Ψ_x was first set to−0.5 MPa for measuring maximum conductivity, $K_{s,max}$. Subsequently, a VC was obtained by repeated K_s measurements, stepwise exposing the segment to more negative pressure until > 90% LC was reached:

$$LC = \left(1 - \frac{K_s}{K_{s,max}}\right) \times 100\% \quad (2)$$

VCs were sigmoidal and fitted to a Weibull function (cumulative distribution function) as:

$$LC/100 = 1 - \exp[-(\Psi_x/B)^C] \quad (3)$$

where the constants were calculated by minimizing RMS error.

The Cavisoft software (version 5.2, University of Bordeaux) was used to control centrifuge speed and for conductivity estimation.

2.3 | OV method

The OV method is based on continuous imaging of the sample when abrupt changes in light reflectance are interpreted as xylem cavitation (Brodribb et al., 2016). A Raspberry Pi microcomputer was used to control and store images produced by a camera, contained within a custom-built clamp that was used to fix the sample in place. The sample field of view was magnified by a ×20 lens and illuminated by LED light source that provided reflected light from the sample surface. Details of the optical system, image capturing, post image processing, and data analysis, as well as an overview of OV method, are present at www.opensourceov.org.

Shoots with a length of 80–90 cm were harvested, wrapped in a black plastic bag, and transferred to the laboratory. Then, the basal ends were recut (by ca. 10 cm in total) under water, and the shoots were allowed to rehydrate for 2 h in buckets filled with water while wrapped in a black plastic bag. After that, the shoots were removed from the water and unwrapped. A small section (rectangle of 2.5 × 1 cm) of the bark and phloem from each collected sample was carefully removed. The exposed xylem was covered with a conductive adhesive gel (Aquasonic Clear; Parker Laboratories Inc.) to reduce heterogeneity in the speed of desiccation across different xylem layers. The camera clamp assembly was positioned to best view the exposed xylem and fixed in place. Images were taken every 5 min. The Ψ_x was measured every 10 min continuously using the PSY1 stem psychrometer (ICT International), which was installed ca. 10–20 cm from the OV clamp. Scholander pressure chamber (Model 1505D; PMS) measurements were taken once a day to validate the psychrometer measurement, which showed a good agreement with the psychrometer method (Supporting Information: Figure S1). A best-fit regression model of the Ψ_x versus time was used to determine the Ψ_x of all the images taken below the Ψ_{tlp} (Supporting Information: Figure S2). Above Ψ_{tlp} the Ψ_x was determined as the nearest psychrometer measurement. The dehydration usually lasted five (summer) or seven (winter) days until cavitation events had ceased (concluded after 24 h with no cavitation events). The image sequences were processed using ImageJ, as described in Hochberg et al. (2017). The degree of cavitation (in %) was expressed as the cumulative number of cavitated pixels at a specific time normalized to the total number of cavitated pixels under full dehydration (Brodribb et al., 2016). These data were used to determine the VCs, which is the percentage of cavitated area as a function of Ψ_x. Weibull function was used to fit the curves when comparing the three methods. However, mean curves, calculated from all the raw individual curves, were used to determine Ψ_{50} for examing its seasonal plasticity.

2.4 | Micro-CT method

The short tracheids of *P. halepensis* (i.e., ~2 mm; David-Schwartz et al., 2016) allow the measurements of cut samples without the risk of artificial cavitation inducement. Small branchlets (1–2 mm in diameter, ~5 cm in length) were removed from the large branch to which the OV sensors were attached. The water potential at sampling was measured by the psychrometer, which was installed ca. 10–20 cm from the OV sensors. Branchlets were covered with a wet paper towel and cut from the large branch. The samples were immediately sealed to prevent water loss by dipping them in hot wax (<60°C) and immediately in ice water. The fixed samples were promptly scanned in the μCT (RX Solutions). Each scan was conducted under a power of 4.8 Watt with a frame rate of 1 image s^{-1} and 1440 images per scan, resulting in a voxel size of 5–8 μm. After the first scan, each sample was cut at the middle of the scanned area to embolize all the tracheids, the cut edge was recovered with parafilm to prevent further dehydration, and the sample was scanned again to account for the branchlet's maximal conductive area (LA_{max}). One slice from each scan was analyzed using ImageJ software

(Schindelin et al., 2012), where the bark, pith tissues and resin ducts were manually cropped out and the air-filled area was quantified just for the xylem tissue using the threshold tool. The degree of cavitation was quantified as:

$$\text{cavitationdegree} = \frac{LA_{nat}}{LA_{max}} \times 100\% \quad (4)$$

where LA_{nat} is the loss of area due to native cavitation shown in the intact scan. Then the VCs was determined by cavitation degree as a function of Ψ_x using Weibull function as stated in cavitron methods.

2.4.1 | Experiment 2—seasonal plasticity of xylem vulnerability

The experiment was conducted on 10-year-old field trees, growing in the Volcani Center, ARO, Israel. The measurements of VCs by OV and cavitron method, Ψ_{midday}, Ψ_{tlp}, and osmotic potential (Ψ_π) were carried out at a 2–6 month intervals from March 2020 to February 2022 (a total of eight time points).

2.5 | Seasonal dynamics of xylem vulnerability

Three to six shoots at each time point, 80–90 cm in length, were excised at noon (11:00 AM–12:00 PM) from the sun-exposed side of the trees, enclosed in a big black plastic bag to avoid water loss, and transferred to the lab. The shoots were allowed to rehydrate for 2 h in buckets filled with tap water while wrapped in a black plastic bag before the dehydration commenced. Vulnerability measurements by the OV method were conducted on shoots, that were formed in the winter of 2020 and were later either 1-year old (March to October 2020), 2-year old (December 2020 to October 2021), or 3-year old (February 2022). At the same time, the OV sensor was attached to the outer edge of the stems; thus, the monitored tissue was mostly made of current-year tracheids. The OV method was used exactly as described in Experiment 1.

Two potential artifacts associated with the OV method were examined and eliminated. First, the OV method examines only the outermost layer of the xylem and thus could result in a deviation from the xylem vulnerability of the whole shoot. To ensure that this is not the case in our study and to strengthen the observation of the OV with a better-tested method, in March and July 2021, VCs were also collected using the cavitron (as described in Experiment 1). Second, the OV method assumes that no xylem embolism are present when the dehydration starts. Accordingly, μCT measurements of native embolism in October 2020 (the end of summer with the lowest Ψ_{midday}) were conducted.

In addition, a short experiment was conducted to examine that the seasonality of OV curves is not a direct function of the Ψ_x. In this experiment, we simulated the Ψ_x reduction of the entire summer in 1 week. VCs were collected in July 2021 for 2-year-old potted seedlings under well-irrigated conditions or exposed to 1 week of dehydration that resulted in a minimal Ψ_x of −2.7 MPa. According to preliminary tests on the well-irrigated seedlings, Ψ_x of −2.7 MPa is the lowest Ψ_x that leads to no cavitation and thus should allow the measurement with the OV method.

Since the VC of December 2020 indicated a less negative Ψ_{50} compared to the VCs of October 2020, we wanted to find if new growth had started. This was done by light microscopy observations of xylem anatomy. Five segments, approximately 2 cm in length and 4-mm in diameter, which were similar in age and diameter to the ones we used for observations on seasonal vulnerability, were soaked in a solution of 70% ethanol for 48 h. Cross-sections of 50 μm thickness were obtained using a sliding microtome (SM2010R; Leica Biosystems). The sections were stained for 30 s with Toluidine Blue O followed by a wash in distilled water. Images of the cross-sections were captured with a digital camera (DS-Ri2; Nikon Instruments) mounted on a Nikon Eclipse Ni microscope (Nikon Instruments).

2.6 | Midday stem water potential (Ψ_{midday}), osmotic potential (Ψ_π), turgor loss point (Ψ_{tlp}) and hydraulic safety margin (HSM)

To estimate the water status of the trees during the course of the season, we measured their Ψ_{midday}, Ψ_π, and Ψ_{tlp}. Ψ_{midday} was measured at noon (11:00 AM–12:00 PM) on twigs from the sun-exposed side of the trees, which were covered with aluminum zipper bags for 30 min before excision, and measured with a Scholander pressure chamber (Model 1505D; PMS). The 30-min leaf coverage was applied to achieve the equilibrium with Ψ_x.

We estimated the Ψ_{tlp} using the Ψ_x~time function (Supporting Information: Figure S2). We assumed that the change in slope is an indication for Ψ_{tlp} because both the lower capacitance and higher stomata conductance above Ψ_{tlp} (Hochberg et al., 2016) are expected to result in much steeper slopes. Since the room temperature was kept constant, the dehydration rate below Ψ_{tlp} was stable, resulting in an easily characterized linear curve that facilitated the determination of Ψ_{tlp}.

Because we evaluated Ψ_{tlp} in a nontraditional method, we tested our values against the needles osmotic potential (Ψ_π). Six 1.5-ml-tubes of needles were collected at each sampling day (from March 2020 to March 2021) and kept frozen at −20°C until analyses. To extract the cell sap, the needles were thawed and centrifuged at 14 000 rpm (MIKRO 120; Hettich) for 2 min. Subsequently, the extracted sap was measured in a vapor pressure osmometer (Vapro 5600; Wescor Inc.). For measurements made using the osmometer, solute concentration was converted to water potential using the van't Hoff equation (Banks and Hirons 2019; Khare 2015) with Ψ_{tlp} (Supporting Information: Figure S3):

$$\Psi_\pi = -CRT \quad (5)$$

C is the solute concentration in mmol kg^{-1}, R is the universal gas constant (8.314472×10^{-6} m^3 MPa K^{-1} mol^{-1}), and T is the temperature in K. Temperature was considered 25°C.

The HSM was defined as the differences between naturally occurring xylem pressures and pressures that would cause hydraulic dysfunction, that is, $\Psi_{midday}-\Psi_{50}$.

2.7 | Statistics

All statistical analyses were done with the SPSS 18.0 statistics package for a personal computer (SPSS) using the 0.05 significance level. Comparisons of more than two groups between all means were made with one-way analysis of variance and the Duncan test. Student's *t* tests were used to compare means between two groups. The values are all given as means ± se.

3 | RESULTS

3.1 | Experiment 1—methods comparison

We found no significant differences among methods in Ψ_{50} (Figure 1, $p > 0.05$), which ranged from −3.81 ± 0.14 MPa in the OV method, through −4.16 ± 0.11 MPa in the cavitron, and down to −4.20 ± 0.36 MPa in the μCT method. Differently, the slope of the OV method was about two to three times as large compared with the other two methods (−60.32 ± 0.90%/MPa in the OV compared with −25.17 ± 3.30%/MPa and −18.83 ± 1.32%/MPa in the μCT and cavitron, respectively; Table 1). Also the Ψ_{12} and Ψ_{88} of the OV method (−3.17 ± 0.12 MPa and −4.40 ± 0.12 MPa, respectively) were significantly different from the microCT (−2.75 ± 0.37 MPa and −5.89 ± 0.41 MPa, respectively) or cavitron (−2.14 ± 0.09 MPa and −6.25 ± 0.24 MPa, respectively; Table 1). The values obtained by the μCT method showed larger variation, probably because the data was collected on separate individual twigs of branches, compared to a single branch in the other methods. Since the Ψ_{50} was the parameter on which all three methods agreed, we decided to focus our analysis of Experiment 2 on Ψ_{50}.

3.2 | Experiment 2—seasonal plasticity of xylem vulnerability

The seasonal dynamics of all measured hydraulic traits (Figure 2a) followed the climatic changes (Figure 2b). The midday xylem water potential (Ψ_{midday}) was the highest at the end of the rain season, with values of −1.72 ± 0.03 MPa in March 2020 and −1.18 ± 0.02 MPa in March 2021, gradually declining to approximately −2.58 MPa in October 2020 and 2021, the end of the dry season. Turgor loss point (Ψ_{tlp}) showed a similar sinusoidal wave pattern as Ψ_{midday}, gradually declining from −2.00 ± 0.24 MPa in March 2020 down to −3.48 ± 0.06 MPa in October 2020, up to −2.17 ± 0.12 MPa in March 2021, down to −3.34 ± 0.06 MPa in October 2021, then back up to −2.10 ± 0.07 MPa in February 2022.

In accordance with our hypothesis, a significant increase was also observed in the cavitation resistance of *P. halepensis* under drying conditions. In 2020, the most notable change was measured in the beginning of the season, with Ψ_{50} shifting from −2.74 ± 0.11 MPa in March to −3.66 ± 0.06 MPa in May (Figure 3, $p = 0.003$). By the end of the dry summer, in October, the cavitation resistance reached its maximum, with Ψ_{50} of −3.96 ± 0.05 MPa. An overall shift of 1.22 MPa in Ψ_{50} occurred over the 20-21 season. Then, a converse trend took place in winter. Less negative Ψ_{50} (−3.36 ± 0.07 MPa, $p = 0.001$) was observed in December, further increasing to −2.99 ± 0.09 MPa in March 2021. A similar trend in cavitation resistance was observed in the following year as well, with Ψ_{50} decreasing from −2.99 ± 0.09 MPa in March to −3.89 ± 0.04 MPa in October and then

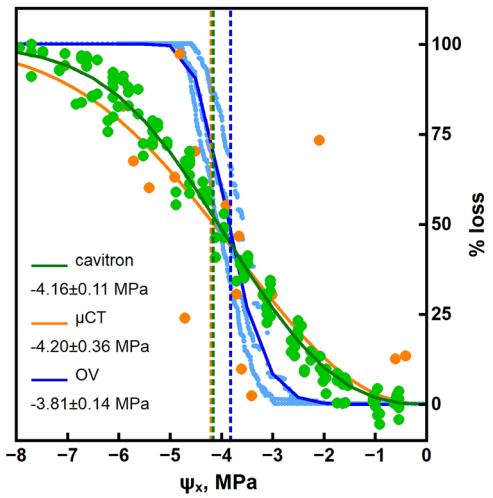

FIGURE 1 Vulnerability curves constructed using the cavitron (green, $n = 5$), μCT (orange) and OV (blue, $n = 3$) methods. Solid lines show the relationships between xylem water potential (Ψ_x) and percentage loss in K_s (cavitron), percentage loss in conductive area (μCT) and percentage loss in pixel area (OV). Each filled dot is a measured datum. Vertical dashed lines mark the point where 50% of the xylem was cavitated (Ψ_{50}). Mean Ψ_{50} ± se measured by the three methods were given beside the legends. For more detailed information regarding vulnerability curves, please see Table 1.

TABLE 1 Values of Ψ_{12}, Ψ_{50}, Ψ_{88} (the points where 12%, 50%, 88% of the xylem were cavitated) and the slope of the vulnerability curves generated from OV, cavitron and μCT methods.

Index	OV	cavitron	μCT
Ψ_{12}, MPa	−3.17 ± 0.12^c	−2.14 ± 0.09^a	−2.75 ± 0.37^b
Ψ_{50}, MPa	−3.81 ± 0.14^a	−4.16 ± 0.11^a	−4.20 ± 0.36^a
Ψ_{88}, MPa	−4.40 ± 0.12^a	−6.25 ± 0.24^b	−5.89 ± 0.41^c
Slope, %/MPa	−60.32 ± 0.90^c	−18.83 ± 1.32^a	25.17 ± 3.30^b

Note: The values are means ± se of three (in OV and μCT) or five repetition (in cavitron). Different letters indicate significant differences at $p = 0.05$ across each row.

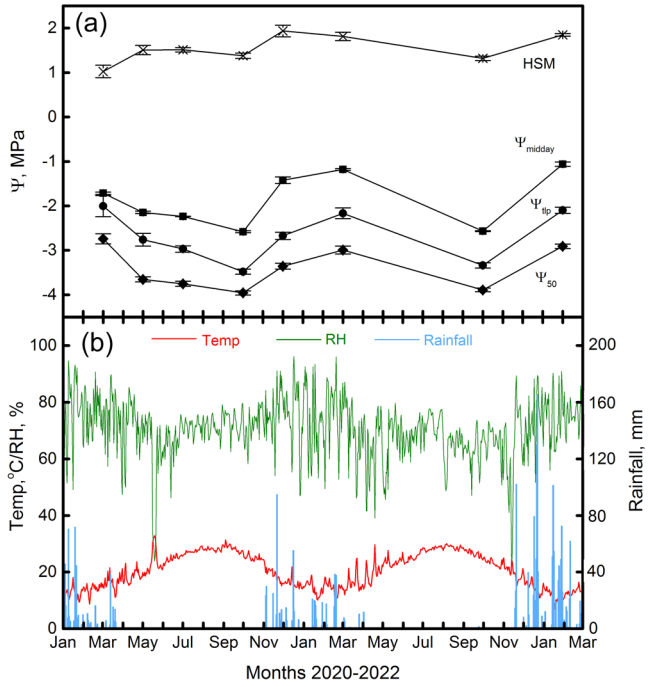

FIGURE 2 (a) Seasonal behavior of midday water potentials (Ψ_{midday}), turgor loss points (Ψ_{tlp}), Ψ_{50} (the points where 50% of the xylem were cavitated), as well as hydraulic safety margin (HSM, Ψ_{midday}–Ψ_{50}) at each sampling month from March 2020 to February 2022. The values are means ± se of three (in Mar. 2020) or six repetitions (in all the other dates). The statistical analysis is presented in Supporting Information: Table S1, while correlations among Ψ_{midday}, Ψ_{tlp} and Ψ_{50} are shown in Supporting Information: Figure S4. (b) Diurnal average air temperature (Temp), relative humidity (RH) and daily rainfall recorded by a weather station 1.8 km away from the location of the sampled trees. ('Bet Dagan' station, https://ims.data.gov.il). [Color figure can be viewed at wileyonlinelibrary.com]

increasing back to −2.91 ± 0.09 MPa in February. The coordinated change of Ψ_{midday},Ψ_{tlp}, and Ψ_{50} ($R^2_{midday\sim tlp}$ = 0.7678, $R^2_{midday\sim 50}$ = 0.7453, $R^2_{tlp\sim 50}$ = 0.9535, Supporting Information: Figure S4) ensured that the plants maintained a positive turgor and an HSM of 1.02 ± 0.14 to 1.93 ± 0.13 MPa throughout the experiment (Figure 2a). Accordingly, the µCT images of the shoots that were collected in October 2020 (before the first rain) showed only a marginal level of native embolism (3%–5%, Figure 4).

Since the OV method 'sees' only the outer part of the xylem and, thus, mostly the newest growth, it does not necessarily represent the entire branch (Brodribb et al., 2017; Gauthey et al., 2020). Accordingly, additional observations in 2021 were done using the cavitron method to confirm that our OV results regarding the seasonal dynamics of Ψ_{50} are also true for the whole branch. A shift of approximately 0.6 MPa in Ψ_{50} was found between the VCs conducted in March (Ψ_{50} = −3.21 ± 0.13 MPa) and July (Ψ_{50} = −3.80 ± 0.06 MPa) (Figure 5). It's important to mention that this shift was not associated with a change in $K_{s,max}$ that did not

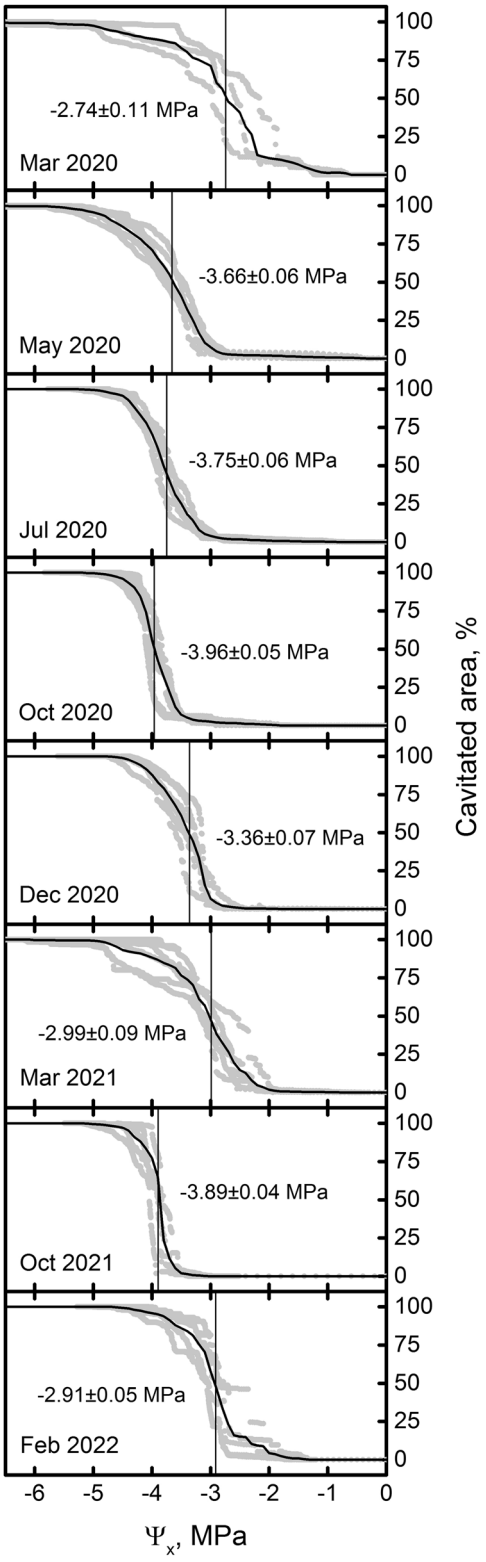

FIGURE 3 Seasonal variation of vulnerability curves (VCs) measured on *Pinus halepensis* using the optical vulnerability method (OV). Individual VCs are shown by gray circles, while respective mean VCs are shown by black solid curves. Vertical solid lines mark the water potential (Ψ_x) where 50% of the xylem was cavitated (Ψ_{50}). Mean Ψ_{50} ± se of each sampling month appears beside the vertical line.

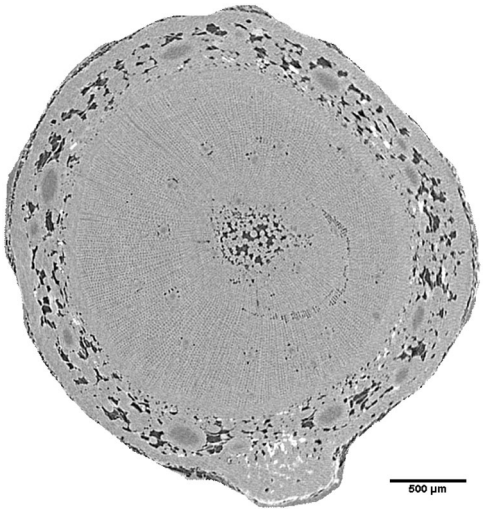

FIGURE 4 An example of visualization of native embolism in the shoot of *Pinus halepensis* harvested in October 2020 (before the first rain) by microcomputed tomography (µCT) method. Black lumina in the xylem indicate air-filled spaces, while gray areas water-filled conduits. In the three shoots we harvested the level of embolism was 3%–5%.

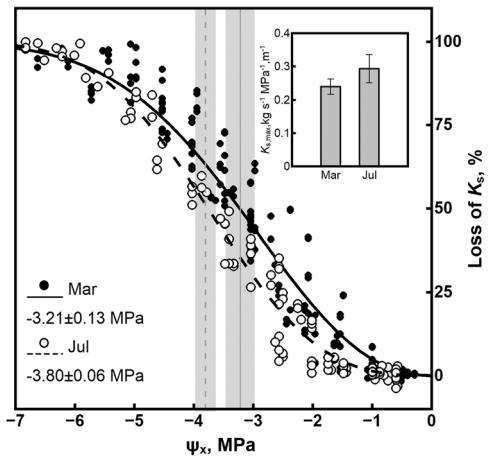

FIGURE 5 Seasonal variation of vulnerability curves (VCs) measured on *Pinus halepensis* using the cavitron method in March and July 2021. The corresponding maximum conductivities measured at −0.5 MPa are shown in the upper right panel. Individual VCs are shown by circles, while mean VCs are shown by the curves. Vertical lines mark the point where 50% of loss of conductivity and shaded areas represent the standard error. $n = 8$ in March and 6 in July. Mean $\Psi_{50} \pm$ se was given respectively beside the legends.

differ between sample times (0.24 ± 0.004 in March and 0.29 ± 0.013 kg s^{-1} MPa^{-1} m^{-1} in July, $p = 0.15$) (Figure 5).

Finally, to provide some insights regarding the source of Ψ_{50} seasonal plasticity, two more measurements were performed. To account for the possibility that the growth of new xylem is in charge of the observed plasticity, a cross-section collected in December confirmed that when Ψ_{50} increased, a substantial amount of new xylem already differentiated (Supporting Information: Figure S5). In addition, our short acclimation experiment showed that the exposure of pines to Ψ_x equivocal to those experienced by the field-grown pines did not change the xylem VC (Supporting Information: Figure S6). The significance of these findings is discussed below.

4 | DISCUSSION

4.1 | Experiment 1—methods comparison

We found that the Ψ_{50} value of *P. halepensis* obtained with the OV method was in close agreement to those obtained by µCT and cavitron (Figure 1). Likewise, Brodribb et al. (2017), Lamarque et al. (2018) and Gauthey et al. (2020) reported that similar estimates of Ψ_{50} were produced by the three techniques for angiosperms and conifers. At the same time, the significantly higher slope of the OV, which was also evident in Brodribb et al. (2017), reminds us that the different methods do not measure the exact same thing (Venturas et al., 2019). Our current understanding regarding the critical role of xylem connectivity in determining its vulnerability (Guan et al., 2021; Wason et al., 2021) could explain why monitoring a small area with conduits at high proximity results in a higher slope as compared with monitoring of the whole cross-section. Furthermore, the fact that the OV requires partial debarking of the stem, could introduce air seeds that are not present under native conditions (Venturas et al., 2019) and thus a different starting point of the VC (Hacke et al., 2022). Finally, because the method were carried on different parts of the shoot (branches for cavitron and OV, branchlets for µCT), and since it is known that xylem structure varies with distance from the branch tip (Hacke et al., 2022; Soriano et al., 2020; Williams et al., 2019), the assumption that the curves should be identical is possibly wrong to begin with. These explanations could also be part of the reasons for the discrepancies between estimates of cavitation resistance derived from the OV and hydraulic methods in previous studies (Pratt et al., 2020; Venturas et al., 2019).

4.2 | Experiment 2—seasonal plasticity of xylem vulnerability

The results supported our hypothesis: the xylem vulnerability of *P. halepensis* shoots was seasonally plastic, adjusting to lower Ψ_{midday} in coordination with the Ψ_{tlp}. Owing to this adjustment, the safety margin was well maintained throughout the year, protecting the shoots from cavitation (Figure 2). The lack of cavitation is also manifested by the seasonally stable K_s values that were measured with the cavitron (Figure 5) and the marginal embolism values (<5%) that were detected with the µCT at the end of the dry season (Figure 4). The significant difference between Ψ_{tlp} and Ψ_{50} (Figure 2) suggests that even under drier conditions significant cavitation is not expected. Typically, when Ψ_{midday} approaches Ψ_{tlp} complete stomatal closure minimizes the transpiration (Brodribb et al., 2003), protecting the plants from further dehydration into cavitating Ψ_{midday}.

It is important to highlight that if we ignore the seasonal adjustment of Ψ_{50}, we might get the wrong impression that the safety margin was eliminated and cavitation had taken place. The Ψ_{midday} decreased to approximately −2.6 MPa in October 2020 (Figure 2), which based on the March Ψ_{tlp} and VC would result in turgor loss and cause about 30% cavitation (Figure 3). Many studies that evaluated native embolism measured the VC at one point of the season and then followed the dynamics of Ψ_x (e.g., Fontes et al., 2018; Hacke and Sauter 1995; Hochberg et al., 2016). Our study shows that such a methodology is potentially erroneous. Since in many cases the VC is constructed in the wet season (to avoid potential native embolism), we believe that many studies have underestimated the safety margin. Such an artifact could be part of the explanation for the many reports of negative safety margins in Mediterranean species (Choat et al., 2012), which seems counter-intuitive from an eco-physiological perspective. The idea of seasonality in Ψ_{50} is so out of the main dogma that many studies (e.g., Benson et al., 2022), including the large hydraulic databases (Choat et al., 2012; Yan et al., 2020), do not report the VC sampling time, making it impossible to estimate the potential extent of such biases.

While out of the main dogma, we speculate that the seasonal plasticity of Ψ_{50} is actually a common phenomenon, especially in plants that experience large changes in water availability between winter and summer. In support, other hydraulic traits that are coordinated with Ψ_{50} (i.e., Ψ_{tlp}) or supposed to mechanically define Ψ_{50} (i.e., xylem anatomy) are seasonally plastic in most species that experience a seasonal drought (Bartlett et al., 2014; Fonti et al., 2010). Furthermore, the current findings add up to six more studies that documented seasonal dynamics in Ψ_{50} (Charrier et al., 2018; Jacobsen et al., 2007; Kolb and Sperry 1999; Sorek et al., 2021, 2022). In total, there are currently 17 species that were documented to exhibit a 1–3 MPa change in Ψ_{50} between, or along, seasons. This little number of species should be weighed against the only 10 species (Jacobsen et al., 2007; Feng et al., 2015; Sorek et al., 2022; Zhang et al., 2018) that showed a constant seasonal Ψ_{50}. Taken together, the current knowledge suggests that the seasonal plasticity of Ψ_{50} is probably common and should to be incorporated into future hydraulic models.

It is difficult to explain the seasonal plasticity of Ψ_{50} because xylem conduits are dead (Choat et al., 2012). It is important to remember that only marginal cavitation values were found in our experiment (Figures 2 and 4), ruling out the possibility that cavitation of the vulnerable tracheids only is in charge of the Ψ_{50} seasonal plasticity (as portrayed in Figure 2 of Mackay et al., 2015). Our acclimation experiment showed that short exposure to low Ψ_x does not change the VC (Supporting Information: Figure S6), implying that the modification is a slow and gradual process. The simplest explanation is that the pine produced more resistant tracheids as summer progressed while vulnerable ones during the wet winter to maximize growth. In support, the cross-section taken in December (Supporting Information: Figure S5) confirmed that by the time Ψ_{50} became less negative, new growth had already taken place. Typically, there is very little growth during summer in Mediterrannean pines (Campelo et al., 2021), theoretically complicating the explanation of the shift between July and October through growth of new xylem. However, it is important to remember that xylem differentiation can be lengthy and the new growth of the early summer could transform into conductive vessels when apparent growth had ceased (Jacobsen et al., 2018; Pratt et al., 2020). At the same time, it is difficult to explain how these new tracheids, which represent only a small proportion of the total conductive xylem, could make such a large impact on Ψ_{50}. We should consider the possibility that since the OV method focus on the outer part of the xylem it augments its importance in determining Ψ_{50}. This could be the reason that the shift between March and July 2020 collected with the OV was ~1 MPa (Figure 3) compared with ~0.6 MPa shift between March and July 2021 collected with the cavitron (Figure 5). Future studies should aim to link the VC dynamics with the seasonal dynamics of xylem conduits differentiation and blockage, as well as the potential shifts in the xylem network connectivity.

Another potential driver for the seasonal plasticity could be the change in xylem sap composition (Losso et al., 2017). Recent findings supported the existence of lipids in the xylem sap (Schenk et al., 2018; Yang et al., 2020), and those could modify the sap's surface tension, potentially changing the Ψ_{50} of the dead tissue. In addition, it is important to remember that structural changes can take place even in a dead conduit. Cell wall thickening and lignification can occur with the assistance of living neighboring cells (Barros et al., 2015; Blokhina et al., 2019). Sorek et al. (2021) suggested that the seasonal change in the Ψ_{50} of grapevine leaves is associated with a seasonal change in the pit membrane thickness of the conductive vessels. Furthermore, While these ideas are yet to offer a mechanistic understanding of seasonal plasticity, they remind us that dead conduits can potentially exhibit plasticity.

5 | CONCLUSION

The findings suggest that the VC of *P. halepensis* is plastic, shifting to more negative Ψ_X during summer. This mechanism enables the trees to maintain a positive safety margin and avoid cavitation. More research is needed to understand how common this plasticity is and what are the mechanisms that drive it. Accounting for the VC seasonal plasticity is important for understanding the actual cavitation danger that plants experience and avoiding potential artefacts. Integrating this plasticity into the basic concepts of plant hydraulics should enable modelers and ecologists to better predict species ability to sustain harsh environments.

ACKNOWLEDGEMENTS

We thank Sylvain Delzon for guidance in Cavitron measurements, Naomi Houminer for anatomy measurements, Smadar Greenstein and Yonatan Sorek for excellent assistance. This work was supported by the Israel Science Foundation, grant no. 1535/19.

CONFLICT OF INTEREST STATEMENT

The authors declare no conflict of interest.

DATA AVAILABILITY STATEMENT

The data that support the findings of this study are available from the corresponding author upon reasonable request.

ORCID

Feng Feng http://orcid.org/0000-0001-9531-6988
Yael Wagner http://orcid.org/0000-0002-2588-9278
Tamir Klein http://orcid.org/0000-0002-3882-8845
Uri Hochberg http://orcid.org/0000-0002-7649-7004

REFERENCES

Anderegg, W.R.L. (2015) Spatial and temporal variation in plant hydraulic traits and their relevance for climate change impacts on vegetation. *New Phytologist*, 205, 1008–1014.

Awad, H., Barigah, T., Badel, E., Cochard, H. & Herbette, S. (2010) Poplar vulnerability to xylem cavitation acclimates to drier soil conditions. *Physiologia Plantarum*, 139, 280–288.

Banks, J.M. & Hirons, A.D. (2019) Alternative methods of estimating the water potential at turgor loss point in *Acer* genotypes. *Plant Methods*, 15, 34.

Barros, J., Serk, H., Granlund, I. & Pesquet, E. (2015) The cell biology of lignification in higher plants. *Annals of Botany*, 115, 1053–1074.

Bartlett, M.K., Zhang, Y., Kreidler, N., Sun, S., Ardy, R., Cao, K. et al. (2014) Global analysis of plasticity in turgor loss point, a key drought tolerance trait. *Ecology Letters*, 17, 1580–1590.

Beikircher, B., Losso, A., Gemassmer, M., Jansen, S. & Mayr, S. (2019) Does fertilization explain the extraordinary hydraulic behaviour of apple trees. *Journal of Experimental Botany*, 70, 1915–1925.

Beikircher, B. & Mayr, S. (2009) Intraspecific differences in drought tolerance and acclimation in hydraulics of *Ligustrum vulgare* and *Viburnum lantana*. *Tree Physiology*, 29, 765–775.

Benson, M.C., Miniat, C.F., Oishi, A.C., Denham, S.O., Domec, J.C., Johnson, D.M. et al. (2022) The xylem of anisohydric *Quercus alba* L. is more vulnerable to embolism than isohydric codominants. *Plant, Cell & Environment*, 45, 329–346.

Blokhina, O., Laitinen, T., Hatakeyama, Y., Delhomme, N., Paasela, T., Zhao, L. et al. (2019) Ray parenchymal cells contribute to lignification of tracheids in developing xylem of Norway spruce. *Plant Physiology*, 181, 1552–1572.

Brodribb, T., Brodersen, C.R., Carriqui, M., Tonet, V., Rodriguez Dominguez, C. & McAdam, S. (2021) Linking xylem network failure with leaf tissue death. *New Phytologist*, 232, 68–79.

Brodribb, T.J., Carriqui, M., Delzon, S. & Lucani, C. (2017) Optical measurement of stem xylem vulnerability. *Plant Physiology*, 174, 2054–2061.

Brodribb, T.J. & Cochard, H. (2009) Hydraulic failure defines the recovery and point of death in water-stressed conifers. *Plant Physiology*, 149, 575–584.

Brodribb, T.J., Holbrook, N.M., Edwards, E.J. & Gutiérrez, M.V. (2003) Relations between stomatal closure, leaf turgor and xylem vulnerability in eight tropical dry forest trees. *Plant, Cell & Environment*, 26, 443–450.

Brodribb, T.J., Skelton, R.P., McAdam, S.A.M., Bienaimé, D., Lucani, C.J. & Marmottant, P. (2016) Visual quantification of embolism reveals leaf vulnerability to hydraulic failure. *New Phytologist*, 209, 1403–1409.

Bucci, S.J., Scholz, F.G., Goldstein, G., Meinzer, F.C., Franco, A.C., Campanello, P.I. et al. (2006) Nutrient availability constrains the hydraulic architecture and water relations of savannah trees. *Plant, Cell and Environment*, 29, 2153–2167.

Campelo, F., Ribas, M. & Gutiérrez, E. (2021) Plastic bimodal growth in a Mediterranean mixed-forest of *Quercus ilex* and *Pinus halepensis*. *Dendrochronologia*, 67, 125836.

Cardoso, A.A., Batz, T.A. & McAdam, S.A.M. (2020) Xylem embolism resistance determines leaf mortality during drought in *Persea americana*. *Plant Physiology*, 182, 547–554.

Cardoso, A.A., Brodribb, T.J., Lucani, C.J., DaMatta, F.M. & McAdam, S.A.M. (2018) Coordinated plasticity maintains hydraulic safety in sunflower leaves. *Plant, Cell & Environment*, 41, 2567–2576.

Charrier, G., Delzon, S., Domec, J.C., Zhang, L., Delmas, C.E.L., Merlin, I. et al. (2018) Drought will not leave your glass empty: low risk of hydraulic failure revealed by long-term drought observations in world's top wine regions. *Science Advances*, 4, 1–10.

Choat, B., Brodersen, C.R. & McElrone, A.J. (2015) Synchrotron X-ray microtomography of xylem embolism in *Sequoia sempervirens* saplings during cycles of drought and recovery. *New Phytologist*, 205, 1095–1105.

Choat, B., Drayton, W.M., Brodersen, C., Matthews, M.A., Shackel, K.A., Wada, H. et al. (2010) Measurement of vulnerability to water stress-induced cavitation in grapevine: a comparison of four techniques applied to a long-vesseled species. *Plant, Cell and Environment*, 33, 1502–1512.

Choat, B., Jansen, S., Brodribb, T.J., Cochard, H., Delzon, S., Bhaskar, R. et al. (2012) Global convergence in the vulnerability of forests to drought. *Nature*, 491, 752–755.

Cochard, H. (2002) A technique for measuring xylem hydraulic conductance under high negative pressures. *Plant, Cell & Environment*, 25, 815–819.

Cochard, H., Damour, G., Bodet, C., Tharwat, I., Poirier, M. & Améglio, T. (2005) Evaluation of a new centrifuge technique for rapid generation of xylem vulnerability curves. *Physiologia Plantarum*, 124, 410–418.

Cochard, H., Delzon, S. & Badel, E. (2015) X-ray microtomography (micro-CT): a reference technology for high-resolution quantification of xylem embolism in trees: A reference method for xylem embolism. *Plant, Cell & Environment*, 38, 201–206.

Corcuera, L., Cochard, H., Gil-Pelegrin, E., & Notivol, E. (2011) Phenotypic plasticity in mesic populations of Pinus pinaster improves resistance to xylem embolism (P50) under severe drought. *Trees*, 25(6), 1033–1042. https://doi.org/10.1007/s00468-011-0578-2

David-Schwartz, R., Paudel, I., Mizrachi, M., Delzon, S., Cochard, H., Lukyanov, V. et al. (2016) Indirect evidence for genetic differentiation in vulnerability to embolism in *Pinus halepensis*. *Frontiers in Plant Science*, 7, 768.

Delzon, S., Douthe, C., Sala, A. & Cochard, H. (2010) Mechanism of water-stress induced cavitation in conifers: bordered pit structure and function support the hypothesis of seal capillary-seeding. *Plant, Cell & Environment*, 33, 2101–2111.

Domec, J.-C., Schafer, K., Oren, R., Kim, H.S., & McCarthy, H.R. (2010) Variable conductivity and embolism in roots and branches of four contrasting tree species and their impacts on whole-plant hydraulic performance under future atmospheric CO_2 concentration. *Tree Physiology*, 30(8), 1001–1015. https://doi.org/10.1093/treephys/tpq054

Ewers, B.E., Oren, R. & Sperry, J.S. (2000) Influence of nutrient versus water supply on hydraulic architecture and water balance in *Pinus taeda*. *Plant, Cell & Environment*, 23, 1055–1066.

Feng, F., Ding, F., & Tyree, M.T. (2015). Investigations concerning cavitation and frost fatigue in clonal 84K poplar using high-resolution cavitron measurements. *Plant Physiology*, 168(1), 144–155. https://doi.org/10.1104/pp.114.256271

Fontes, C.G., Dawson, T.E., Jardine, K., McDowell, N., Gimenez, B.O., Anderegg, L. et al. (2018) Dry and hot: the hydraulic consequences of a climate change-type drought for Amazonian trees. *Philosophical Transactions of the Royal Society, B: Biological Sciences*, 373, 20180209.

Fonti, P., von Arx, G., García-González, I., Eilmann, B., Sass-Klaassen, U., Gärtner, H. et al. (2010) Studying global change through investigation of the plastic responses of xylem anatomy in tree rings. *New Phytologist*, 185, 42–53.

Gauthey, A., Peters, J.M.R., Carins-Murphy, M.R., Rodriguez-Dominguez, C.M., Li, X., Delzon, S. et al. (2020) Visual and hydraulic techniques produce similar estimates of cavitation resistance in woody species. *New Phytologist*, 228, 884–897.

Guan, X., Pereira, L., McAdam, S.A.M., Cao, K.F. & Jansen, S. (2021) No gas source, no problem: proximity to pre-existing embolism and segmentation affect embolism spreading in angiosperm xylem by gas diffusion. *Plant, Cell & Environment*, 44, 1329–1345.

Hacke, U. & Sauter, J.J. (1995) Vulnerability of xylem to embolism in relation to leaf water potential and stomatal conductance in *Fagus sylvatica* f. *purpurea* and *Populus balsamifera*. *Journal of Experimental Botany*, 46, 1177–1183.

Hacke, U.G., Jacobsen, A.L. & Pratt, R.B. (2022) Vessel diameter and vulnerability to drought-induced embolism: within-tissue and across-species patterns and the issue of survivorship bias. *IAWA Journal*, 1–16. https://doi.org/10.1163/22941932-bja10107

Hacke, U.G., Plavcova, L., Almeida-Rodriguez, A., King-Jones, S., Zhou, W. & Cooke, J.E.K. (2010) Influence of nitrogen fertilization on xylem traits and aquaporin expression in stems of hybrid poplar. *Tree Physiology*, 30, 1016–1025.

Hammond, W.M., Yu, K., Wilson, L.A., Will, R.E., Anderegg, W.R.L. & Adams, H.D. (2019) Dead or dying? Quantifying the point of no return from hydraulic failure in drought-induced tree mortality. *New Phytologist*, 223, 1834–1843.

Harvey, H.P. & Van Den Driessche, R. (1997) Nutrition, xylem cavitation and drought resistance in hybrid poplar. *Tree Physiology*, 17, 647–654.

Harvey, H.P. & Van Den Driessche, R. (1999) Nitrogen and potassium effects on xylem cavitation and water-use efficiency in poplars. *Tree Physiology*, 19, 943–950.

Herrera, J.C., Calderan, A., Gambetta, G.A., Peterlunger, E., Forneck, A., Sivilotti, P. et al. (2022) Stomatal responses in grapevine become increasingly more tolerant to low water potentials throughout the growing season. *The Plant Journal*, 109, 804–815.

Hochberg, U., Herrera, J.C., Cochard, H. & Badel, E. (2016) Short-time xylem relaxation results in reliable quantification of embolism in grapevine petioles and sheds new light on their hydraulic strategy. *Tree Physiology*, 36, 748–755.

Hochberg, U., Windt, C.W., Ponomarenko, A., Zhang, Y.J., Gersony, J., Rockwell, F.E. et al. (2017) Stomatal closure, basal leaf embolism, and shedding protect the hydraulic integrity of grape stems. *Plant Physiology*, 174, 764–775.

Jacobsen, A.L., Pratt, R.B., Davis, S.D. & Ewers, F.W. (2007) Cavitation resistance and seasonal hydraulics differ among three arid Californian plant communities. *Plant, Cell & Environment*, 30, 1599–609.

Jacobsen, A.L., Pratt, R.B., Davis, S.D. & Tobin, M.F. (2014) Geographic and seasonal variation in chaparral vulnerability to cavitation. *Madroño*, 61, 317–327.

Jacobsen, A.L., Valdovinos-Ayala, J. & Pratt, R.B. (2018) Functional lifespans of xylem vessels: development, hydraulic function, and post-function of vessels in several species of woody plants. *American Journal of Botany*, 105, 142–150.

Kaack, L., Weber, M., Isasa, E., Karimi, Z., Li, S., Pereira, L. et al. (2021) Pore constrictions in intervessel pit membranes provide a mechanistic explanation for xylem embolism resistance in angiosperms. *New Phytologist*, 230, 1829–1843.

Khare, R. (2015) A new approach to derivation of Van't Hoff equation for osmotic pressure of a dilute solution. *American International Journal of Research in Science, Technology, Engineering & Mathematics*, 11, 172–174.

Klein, T., Di Matteo, G., Rotenberg, E., Cohen, S. & Yakir, D. (2013) Differential ecophysiological response of a major Mediterranean pine species across a climatic gradient. *Tree Physiology*, 33, 26–36.

Kolb, U. & Sperry, U. (1999) Transport constraints on water use by the Great Basin shrub, *Artemisia Tridentata*. *Plant, Cell & Environment*, 22, 925–935.

Kursar, T.A., Engelbrecht, B.M.J., Burke, A., Tyree, M.T., El Omari, B. & Giraldo, J.P. (2009) Tolerance to low leaf water status of tropical tree seedlings is related to drought performance and distribution. *Functional Ecology*, 23, 93–102.

Ladjal, M., Huc, R. & Ducrey, M. (2005) Drought effects on hydraulic conductivity and xylem vulnerability to embolism in diverse species and provenances of Mediterranean cedars. *Tree Physiology*, 25, 1109–1117.

Lamarque, L.J., Corso, D., Torres-Ruiz, J.M., Badel, E., Brodribb, T.J., Burlett, R. et al. (2018) An inconvenient truth about xylem resistance to embolism in the model species for refilling *Laurus nobilis* L. *Annals of Forest Science*, 75, 88.

Lamy, J.B., Delzon, S., Bouche, P.S., Alia, R., Vendramin, G.G., Cochard, H. et al. (2014) Limited genetic variability and phenotypic plasticity detected for cavitation resistance in a Mediterranean pine. *New Phytologist*, 201, 874–886.

Lemoine, D., Cochard, H. & Granier, A. (2002) Within crown variation in hydraulic architecture in beech (*Fagus sylvatica* L): evidence for a stomatal control of xylem embolism. *Annals of Forest Science*, 59, 19–27.

López, R., López de Heredia, U., Collada, C., Cano, F.J., Emerson, B.C., Cochard, H., & Gil, L. (2013) Vulnerability to cavitation, hydraulic efficiency, growth and survival in an insular pine (Pinus canariensis). *Annals of Botany*, 111(6), 1167–1179. https://doi.org/10.1093/aob/mct084

Losso, A., Beikircher, B., Dämon, B., Kikuta, S., Schmid, P. & Mayr, S. (2017) Xylem sap surface tension may be crucial for hydraulic safety. *Plant Physiology*, 175, 1135–1143.

Mackay, D.S., Roberts, D.E., Ewers, B.E., Sperry, J.S., McDowell, N.G. & Pockman, W.T. (2015) Interdependence of chronic hydraulic dysfunction and canopy processes can improve integrated models of tree response to drought. *Water Resources Research*, 51, 6156–6176.

Maherali, H. & DeLucia, E.H. (2000) Xylem conductivity and vulnerability to cavitation of ponderosa pine growing in contrasting climates. *Tree Physiology*, 20, 859–867.

Martorell, S., Medrano, H., Tomàs, M., Escalona, J.M., Flexas, J. & Diaz-Espejo, A. (2015) Plasticity of vulnerability to leaf hydraulic dysfunction during acclimation to drought in grapevines: an osmotic-mediated process. *Physiologia Plantarum*, 153, 381–391.

Mayr, S., Wolfschwenger, M. & Bauer, H. (2002) Winter-drought induced embolism in Norway spruce (*Picea abies*) at the Alpine timberline. *Physiologia Plantarum*, 115, 74–80.

McDowell, N., Pockman, W.T., Allen, C.D., Breshears, D.D., Cobb, N., Kolb, T. et al. (2008) Mechanisms of plant survival and mortality during drought: why do some plants survive while others succumb to drought? *New Phytologist*, 178, 719–739.

Pivovaroff, A.L., Burlett, R., Lavigne, B., Cochard, H., Santiago, L.S. & Delzon, S. (2016) Testing the 'microbubble effect' using the cavitron technique to measure xylem water extraction curves. *AoB Plants*, 8, 1–10.

Plavcová, L. & Hacke, U.G. (2012) Phenotypic and developmental plasticity of xylem in hybrid poplar saplings subjected to experimental drought, nitrogen fertilization, and shading. *Journal of Experimental Botany*, 63, 6481–6491.

Plavcová, L., Hacke, U.G., Almeida-Rodriguez, A.M., Li, E. & Douglas, C.J. (2013) Gene expression patterns underlying changes in xylem structure and function in response to increased

nitrogen availability in hybrid poplar. *Plant, Cell & Environment*, 36, 186–199.

Pratt, R.B., Castro, V., Fickle, J.C. & Jacobsen, A.L. (2020) Embolism resistance of different aged stems of a California oak species (*Quercus douglasii*): optical and microCT methods differ from the benchtop-dehydration standard. *Tree Physiology*, 40, 5–18.

Schenk, H.J., Espino, S., Rich-Cavazos, S.M. & Jansen, S. (2018) From the sap's perspective: the nature of vessel surfaces in angiosperm xylem. *American Journal of Botany*, 105, 172–185.

Schenk, H.J., Steppe, K. & Jansen, S. (2015) Nanobubbles: a new paradigm for airseeding in xylem. *Trends in Plant Science*, 20, 199–205.

Schindelin, J., Arganda-Carreras, I., Frise, E., Kaynig, V., Longair, M., Pietzsch, T. et al. (2012) Fiji: an open-source platform for biological-image analysis. *Nature Methods*, 9, 676–682.

Schoonmaker, A.L., Hacke, U.G., LandhäUsser, S.M., Lieffers, V.J. & Tyree, M.T. (2010) Hydraulic acclimation to shading in boreal conifers of varying shade tolerance. *Plant, Cell & Environment*, 33, 382–393.

Skelton, R.P., Brodribb, T.J., McAdam, S.A.M. & Mitchell, P.J. (2017) Gas exchange recovery following natural drought is rapid unless limited by loss of leaf hydraulic conductance: evidence from an evergreen woodland. *New Phytologist*, 215, 1399–1412.

Sorek, Y., Greenstein, S. & Hochberg, U. (2022) Seasonal adjustment of leaf embolism resistance and its importance for hydraulic safety in deciduous trees. *Physiologia Plantarum*, 174, e13785.

Sorek, Y., Greenstein, S., Netzer, Y., Shtein, I., Jansen, S. & Hochberg, U. (2021) An increase in xylem embolism resistance of grapevine leaves during the growing season is coordinated with stomatal regulation, turgor loss point and intervessel pit membranes. *New Phytologist*, 229, 1955–1969.

Soriano, D., Echeverría, A., Anfodillo, T., Rosell, J.A. & Olson, M.E. (2020) Hydraulic traits vary as the result of tip-to-base conduit widening in vascular plants. *Journal of Experimental Botany*, 71, 4232–4242.

Stiller, V. (2009) Soil salinity and drought alter wood density and vulnerability to xylem cavitation of baldcypress (*Taxodium distichum* (L.) Rich.) seedlings. *Environmental and Experimental Botany*, 67, 164–171.

Turner, N.C. (1988) Measurement of plant water status by the pressure chamber technique. *Irrigation Science*, 9, 289–308.

Tyree, M.T. & Zimmermann, M.H. (2002) *Xylem Structure and the Ascent of Sap*, Ed 2. Springer-Verlag.

Unterholzner, L., Carrer, M., Bär, A., Beikircher, B., Dämon, B., Losso, A. et al. (2020) *Juniperus communis* populations exhibit low variability in hydraulic safety and efficiency. *Tree Physiology*, 40, 1668–1679.

Venturas, M.D., Pratt, R.B., Jacobsen, A.L., Castro, V., Fickle, J.C. & Hacke, U.G. (2019) Direct comparison of four methods to construct xylem vulnerability curves: differences among techniques are linked to vessel network characteristics. *Plant, Cell & Environment*, 42, 2422–2436.

Villagra, M., Campanello, P.I., Montti, L. & Goldstein, G. (2013) Removal of nutrient limitations in forest gaps enhances growth rate and resistance to cavitation in subtropical canopy tree species differing in shade tolerance. *Tree Physiology*, 33, 285–296.

Von Arx, G., Archer, S.R. & Hughes, M.K. (2012) Long-term functional plasticity in plant hydraulic architecture in response to supplemental moisture. *Annals of Botany*, 109, 1091–1100.

Wason, J., Bouda, M., Lee, E.F., McElrone, A.J., Phillips, R.J., Shackel, K.A. et al. (2021) Xylem network connectivity and embolism spread in grapevine (*Vitis vinifera L.*). *Plant Physiology*, 186, 373–387.

Wheeler, J.K., Huggett, B.A., Tofte, A.N., Rockwell, F.E. & Holbrook, N.M. (2013) Cutting xylem under tension or supersaturated with gas can generate PLC and the appearance of rapid recovery from embolism. *Plant, Cell and Environment*, 36, 1938–1949.

Williams, C.B., Anfodillo, T., Crivellaro, A., Lazzarin, M., Dawson, T.E. & Koch, G.W. (2019) Axial variation of xylem conduits in the Earth's tallest trees. *Trees*, 33, 1299–1311.

Yan, C.L., Ni, M.Y., Cao, K.F. & Zhu, S.D. (2020) Leaf hydraulic safety margin and safety-efficiency trade-off across angiosperm woody species. *Biology Letters*, 16, 20200456.

Yang, J., M Michaud, J., Jansen, S., Schenk, H.J. & Zuo, Y.Y. (2020) Dynamic surface tension of xylem sap lipids. *Tree Physiology*, 40, 433–444.

Zhang, W., Feng, F. & Tyree, M.T. (2018) Seasonality of cavitation and frost fatigue in *Acer mono* maxim. *Plant, Cell & Environment*, 41, 1278–1286.

SUPPORTING INFORMATION

Additional supporting information can be found online in the Supporting Information section at the end of this article.

How to cite this article: Feng, F., Wagner, Y., Klein, T. & Hochberg, U. (2023) Xylem resistance to cavitation increases during summer in *Pinus halepensis*. *Plant, Cell & Environment*, 46, 1849–1859. https://doi.org/10.1111/pce.14573